Lawrence Berkeley National Laboratory
Recent Work

Title

STRESS INDUCED MICROCRACK . GEOMETRY AT FAILURE IN UNCONFINED AND CONFINED AXIAL COMPRESSIVE TESTS

Permalink

https://escholarship.org/uc/item/4r52x68p

Authors

Zheng, Z.
Myer, L.R.
Cook, N.G.W.

Publication Date

1989

eScholarship.org Powered by the California Digital Library
University of California

LBL-26595

Lawrence Berkeley Laboratory
UNIVERSITY OF CALIFORNIA

EARTH SCIENCES DIVISION

RECEIVED
LAWRENCE
BERKELEY LABORATORY
MAY 18 1989
LIBRARY AND
DOCUMENTS SECTION

To be presented at the 30th U.S. Symposium on
Rock Mechanics, Morgantown, WV, June 19–22, 1989

Stress Induced Microcrack Geometry at Failure in Unconfined and Confined Axial Compressive Tests

Z. Zheng, L.R. Myer, and N.G.W. Cook

January 1989



LBL-26595

Prepared for the U.S. Department of Energy under Contract Number DE-AC03-76SF00098.

DISCLAIMER

This document was prepared as an account of work sponsored by the United States Government. While this document is believed to contain correct information, neither the United States Government nor any agency thereof, nor the Regents of the University of California, nor any of their employees, makes any warranty, express or implied, or assumes any legal responsibility for the accuracy, completeness, or usefulness of any information, apparatus, product, or process disclosed, or represents that its use would not infringe privately owned rights. Reference herein to any specific commercial product, process, or service by its trade name, trademark, manufacturer, or otherwise, does not necessarily constitute or imply its endorsement, recommendation, or favoring by the United States Government or any agency thereof, or the Regents of the University of California. The views and opinions of authors expressed herein do not necessarily state or reflect those of the United States Government or any agency thereof or the Regents of the University of California.

LBL-26595

STRESS INDUCED MICROCRACK GEOMETRY AT FAILURE IN UNCONFINED AND CONFINED AXIAL COMPRESSIVE TESTS

Z. Zheng,[*†] *L. R. Myer,*[†] *and N. G. W. Cook*[*†]

[*]Department of Materials Science & Mineral Engineering
University of California

and

[†]Earth Sciences Division
Lawrence Berkeley Laboratory
1 Cyclotron Road
Berkeley, California 94720

January 1989

This work was supported by the Director, Office of Energy Research, Office of Basic Energy Sciences, Engineering, Mathematics, and Geosciences Division, of the U.S. Department of Energy under Contract No. DE-AC03-76SF00098.

ABSTRACT: Cylindrical specimens of Indiana limestone have been tested in uniaxial, confined and partially confined compression. A low melting point metal alloy was used as a pore fluid. At the stress of interest this alloy was solidified in place to preserve the stress-induced microcracks. Optical and electron micrographs of cross sections from the specimens were used to study the density, orientation, thickness and mechanism of these microcracks as a function of confinement.

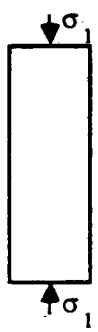
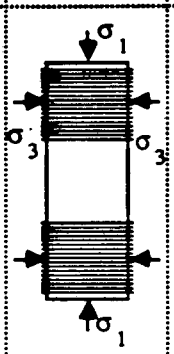
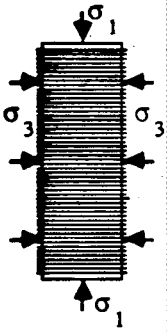
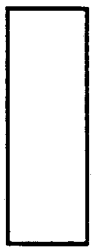
INTRODUCTION

Rock specimens tested in compression display initial consolidation, linear elastic and then strain hardening deformation up to the peak stress, followed by strain softening in the post failure regime. The non-linear modes of deformation and dilatation are probably due to the formation of extensile microcracks under differential compression (Brace et al. 1966, Scholz, 1968 and Rao and Ramana, 1974). Many theories of extensile microcrack generation and propagation in compression have been proposed, including the sliding crack mechanism (Hoek and Bieniawski, 1965, Brace et al., 1966, Horri and Nemat-Nasser, 1985, Ashby and Hallam, 1986 and Kemeny and Cook, 1987; the generation of microcracks by local tensile stresses resulting from mismatched elastic properties between grains, or indentation of one grain by another (Dey and Wang,1981); tensile stresses inside a grain due to Brazilian type loading (Gallagher et al., 1974), and microcracks from tensile stresses adjacent to pores (Sammis and Ashby, 1986). Detailed measurements of microcrack populations in laboratory specimens have been made (Peng and Johnson, 1972, Hallbauer et al., 1973, Gallagher et al., 1974, Olsson, 1974, Hadley, 1976 and Tapponier and Brace, 1976, etc.), but mostly on crystalline rocks.

The observation of microcracks in rocks as they exist under load is very difficult because existing microcracks may close and new microcracks may be generated by unloading and the preparation of sections. To distinguish microcracks produced during loading from those produced by unloading, we have used a low melting point metal alloy -- Cerrosafe® -- which is liquid at 87°C, as a pore fluid. The metal alloy can be solidified at any stage of an experiment to preserve the microcracks as they exist under loading and to distinguish these microcracks from those initiated later. At a pore pressure of 10MPa the liquid metal penetrates openings as small as 0.08μm.

Specimens of Indiana limestone were tested in uniaxial, partially confined and confined compression, and complete stress-strain curves were recorded. Observations of microcracks were made on polished sections of these specimens using optical and scanning electron microscopy at different magnification levels. Statistical data on the distributions of microcrack density, crack lengths, thickness and orientation are presented. The results show that the microcracks are mostly aligned in the direction of the maximum compressive stress. The distributions of crack length, density and thickness depend strongly on the

confining stresses. The volumetric strain and the final porosity of the rock specimens were measured and found to depend on the confining stresses.

Specimen #	1	2	3	4	5	6
Confinement Conditions						
Strain Softening?	Y *	Y	N	N	N	N
Maximum Stress (MPa)	76	90	110	130	145	20
Porosity	13.21%	9.99% 11.74% 9.11%	10.06%	10.01%	8.80%	10.31%
Crack Density	0.87/mm^2	0.58/mm^2	0.59/mm^2	0.60/mm^2	0.34/mm^2	0
Crack Length Distribution	L=.68mm S=.65mm S/L=.96	L=.58mm S=.50mm S/L=.86	L=.46mm S=.27mm S/L=.59	L=.42mm S=.21mm S/L=.50	L=.39mm S=.16mm S/L=.41	N/A
Crack Thickness Distribution	t =.01mm S=.019mm S/t=1.9	t = .008mm S=.015mm S/t=1.875	t = .007mm S=.013mm S/t=1.857	t = .004mm S=.004mm S/t=1	t = .004mm S=.004mm S/t=1	N/A
Crack Orientation (Degrees)	θ =5.6 S =10.5	θ =0.9 S =14.2	θ =6.8 S =14.1	θ =4.5 S =7.9	θ =7.7 S =15.2	N/A

* Y - yes; N - no; L = average length; t =average thickness

S = standard deviation, assuming normal distribution

Table 1. Summary of test conditions and results for specimens of Indiana limestone confined with stainless steel wire.

EXPERIMENTAL AND OBSERVATION PROCEDURES

Cylindrical specimens of Indiana limestone were tested in five different conditions. Table 1 lists all the information about the specimens and the results of the tests. The specimens, 73mm long and 25.4mm in diameter, were cored from the same block of rock, with the axes of the specimens perpendicular to the bedding. Confining stress was applied by stainless steel wire wound around the rock specimens. The ends of some of the specimens were wrapped with pre-tensioned stainless steel wire to act as a crack arrestor near the ends of the specimens adjacent to the loading plate, and to ensure that the tests would remain stable even for Class II behavior (Wawersik and Fairhurst, 1970). On other specimens continuous wrapping along the full length was done to achieve triaxial confinement. Different degrees of confinement could be achieved by varying the pitch (larger than the diameter of the wire) and pre-tension in the wire. Test conditions are summarized in table 1. Specimen #1 was tested under uniaxial compression, specimen #2 was tested with one third of its length at each end confined and the central third unconfined, specimen #3 was tested triaxially with low confining stress, specimen #4 was under a confining stress twice of that on #3 and specimen #5 was under the highest confining stress. Specimen #6, which is used as a reference specimen, was loaded uniaxially up to one fourth of the compressive strength of the rock. The specimens were submerged in molten metal as a pore fluid at a pressure of 10MPa. The loading was performed in a servo-controlled stiff testing machine, so that the complete stress-strain curves cloud be recorded.

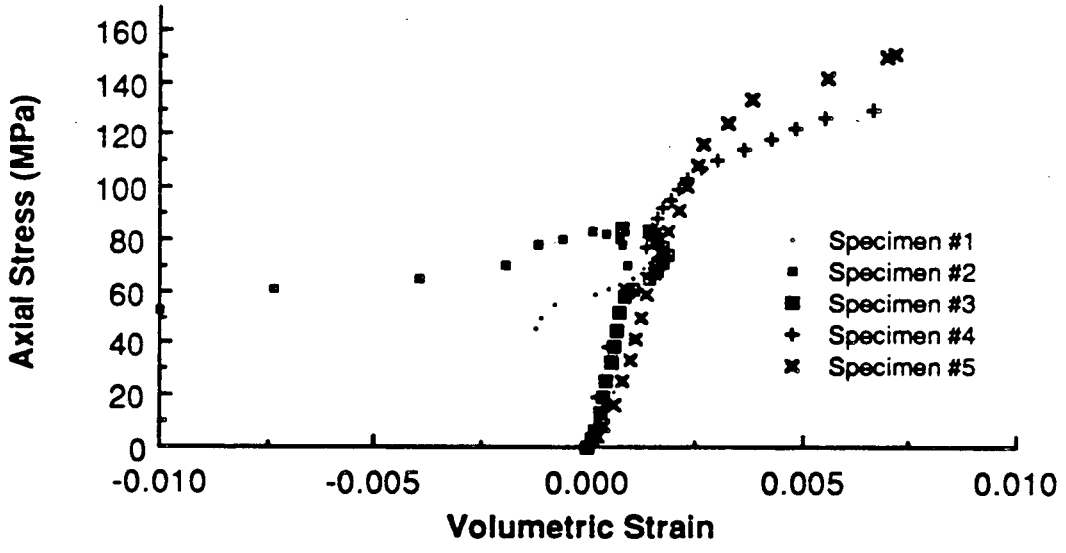


Figure 1. Stress vs. volumetric strain curves for five different loading conditions. Specimen #1 was under uniaxial compression. The central third of specimen #2 was in uniaxial compression and the ends were confined. Specimens #3 to #5 were subjected to increasing amounts of confining stress.

Figure 1 shows the recorded axial stress vs.volumetric strain curves for the five different stress conditions. Each test specimen was then sectioned along its axis, ground and polished for microscopic examination and photography. The microcracks were traced from micrographs of 12.5 times magnification taken from the middle sections of the specimens. The micrographs were divided into sections equivalent to 1.6mm × 1.6mm on the specimen. In each small section the number of microcracks, their lengths, thicknesses and orientations were recorded. Other micrographs with magnifications of up to 3600 times were taken to study the details at crack tips and to look for very small microcracks. The final porosities of the specimens were carefully measured and compared to that of specimen #6 to examine the effect of confining stress on dilatation and pore collapse.

OBSERVATION AND STATISTICAL RESULTS

1. Microcrack Orientations and Origins

Most of the microcracks were observed to be extensile and subparallel to the direction of the maximum compressive stress. In all the specimens tested, the fractures were found to be within 15 degrees of the maximum compressive stress direction. The average orientation of all the microcracks, obtained from the absolute values (ignoring sign) of the angles from the direction of axial compression, is 5 degrees with a standard deviation of 12 degrees. Most of the cracks initially start at some nonzero angle to the direction of maximum compression, turning to propagate along the direction of axial compression throughout most of their length. Details of the tips of microcracks show that they turn into the direction of one of the slip planes of the grains just before the microcracks were fully arrested.

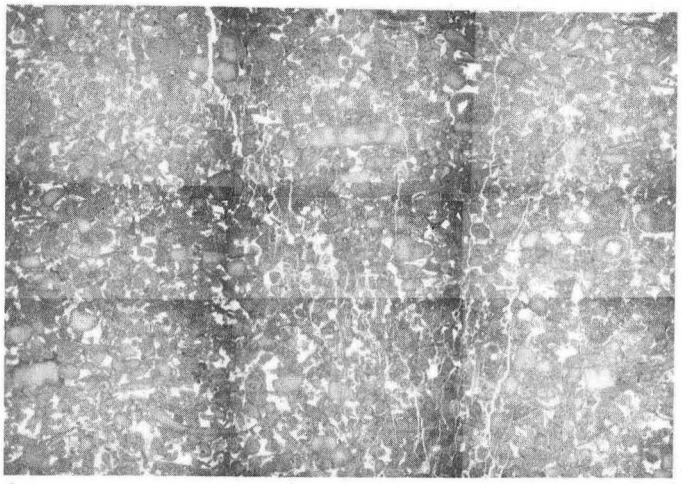
The microcracks appear to have been generated by six different mechanisms. Many microcracks are caused by the bending of long, beam-like grains parallel to the bedding. Microcracks generated from pores or very porous grains, as a result of tension around these voids or soft inclusions, are frequently observed. Sliding cracks are found to start at grain boundaries and then propagate in the direction of the maximum compression into intact grains. Cracks generated from grain boundaries can also propagate along the boundary, particularly when the boundary is almost parallel to the direction of maximum compression. Many grains have point contacts with other grains and cracks are generated as the result of point loading. Grains loaded across their diameter, as in a Brazilian test, are also found in the specimens. Microcracks of this sort are aligned with the line connecting the loading points, and, these lines are not necessarily subparallel to the axial compression. When the weak plane inside a crystal grain is subparallel to the direction of loading, slipping along the weak planes is found to be the mechanism of the microcrack generation in the grain.

2. Microcrack Density

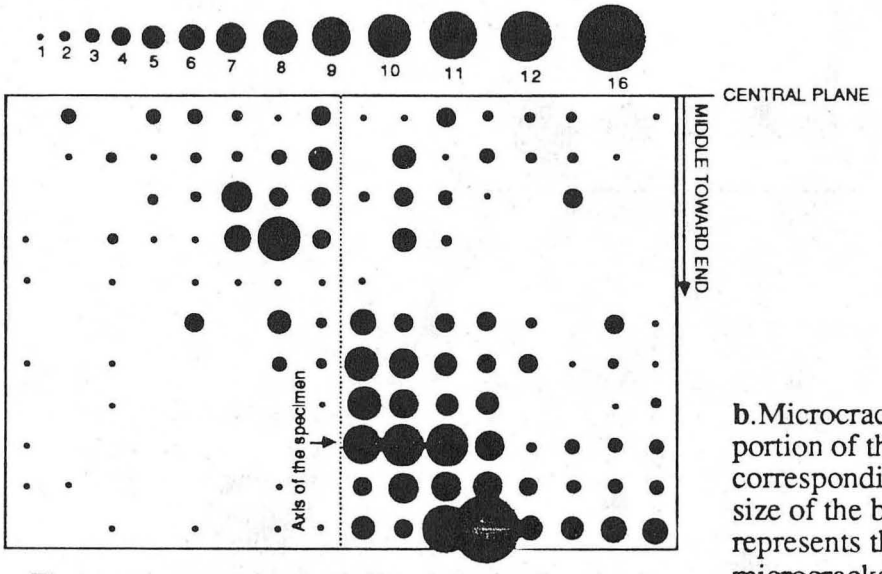
The density distributions of the microcracks are listed in Table 1. Specimen #1 (Figure 2a,b), subjected to uniaxial compression, had the highest crack density. Specimen #5 (Figure 3a,b), which was under the greatest confining stress, starting at 7MPa, has the lowest crack density, 0.34 cracks/mm^2. Specimen #3 and #4 with low confining stresses, have almost the same crack density, 0.6 cracks/mm^2. Specimen #2, which was subjected to a confining stress starting at 7MPa over each end and uniaxial compression over the center, has a crack density of 0.67 cracks/mm^2 in the central portion, and a density of less than 0.05 cracks/mm^2 in its confined portion yielding an overall average of 0.58 cracks/mm^2. In order to detect microcracks not visible on the micrographs at 12.5× magnification, higher magnification micrographs (up to 3600×) were taken using the SEM. However, very few additional microcracks were observed at these higher magnifications. Our study of a clastic rock with soft mineral grains yielded crack densities less than a tenth of those found by Hadley (1976) in Westerly granite which has microcrack density up to 8 cracks/mm^2. Note that the liquid metal injection technique used enables us to study cracks down to 0.1μm thick.

3. Microcrack Length distribution

The distributions of the microcrack lengths have strong dependence on confining stress. In specimen #1, most of the microcracks propagated to lengths of about 1-3 grain diameters with an average length of 0.68mm and stopped. Figure 2c shows the length and orientation distribution plot of microcracks in specimen #1. With increasing confining stress, the average lengths of the microcracks and the ratio of their standard deviation to average lengths decrease as shown on Table 1. Specimen #5, which was subjected to the greatest confining stress, has an average microcrack length of 0.39mm. The distribution of length and orientation for the microcracks in specimen #5 is plotted in figure 3c.

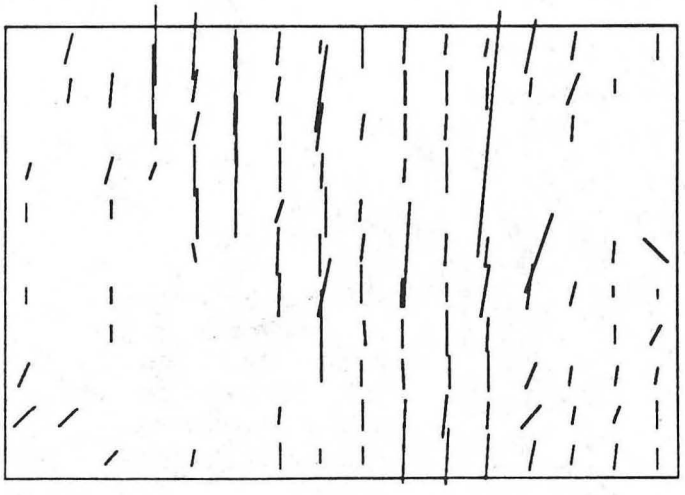


a.Micrograph of the central portion of the specimen obtained from an optical microscope. The horizontal width of the micrograph is 25.4mm and the direction of axial compression is vertical.



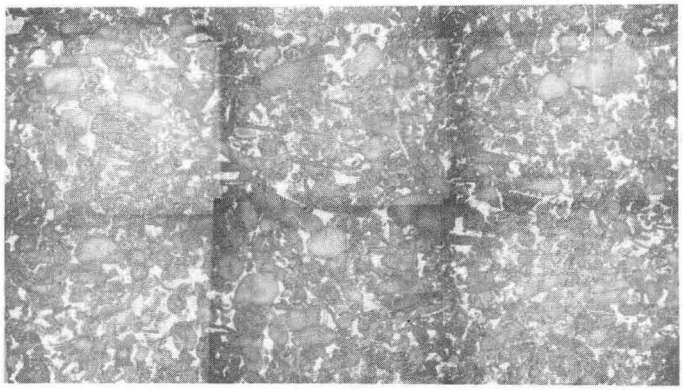
• The numbers underneath the dots are the numbers of microcracks per 2.56mm^2

b.Microcrack density in the portion of the specimen corresponding to **a**. The size of the black dots represents the number of microcracks in a 1.6mm × 1.6mm square.

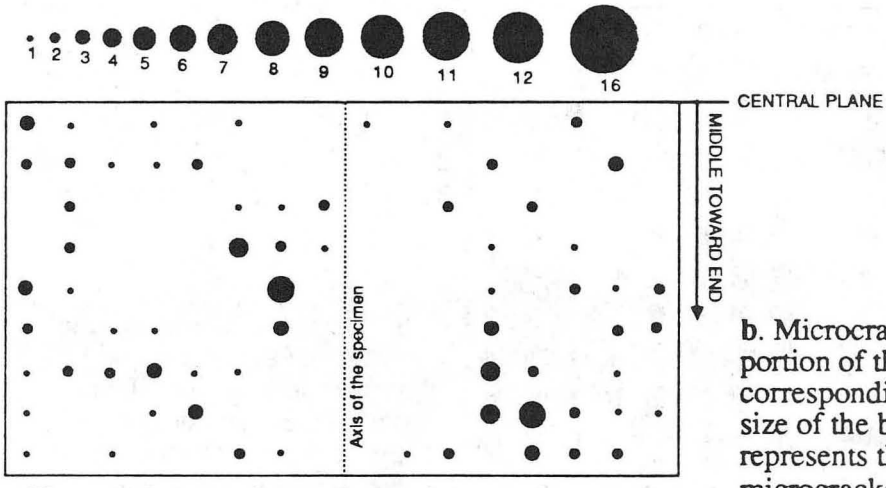


c. Microcrack length and orientation for the same portion of the specimen. The lengths and orientations are the averages in each 1.6mm × 1.6mm square.

Figure 2. Micrograph and crack statistics of specimen #1, which was uniaxially compressed and failed along a shear band.

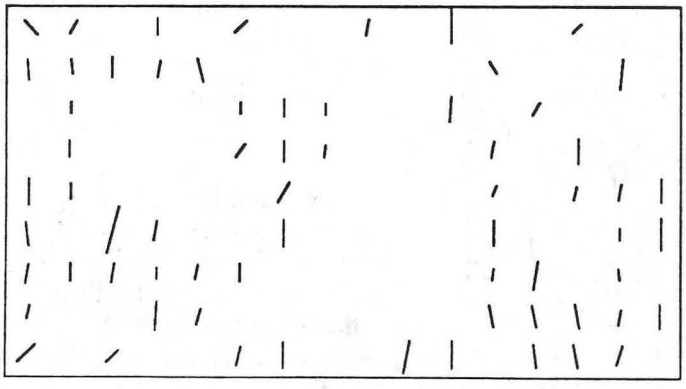


a. Micrograph of the central portion of the specimen obtained from an optical microscope. The horizontal width of the micrograph is 25.4mm and the direction of axial compression is vertical.



• The numbers underneath the dots are the numbers of microcracks per 2.56mm^2

b. Microcrack density in the portion of the specimen corresponding to **a**. The size of the black dots represents the number of microcracks in a 1.6mm × 1.6mm square.



c. Microcracks length and orientation for the same portion of the specimen. The lengths and orientations are the averages in each 1.6mm × 1.6mm square.

Figure 3. Micrograph and crack statistics of specimen #5, which was subjected to the greatest confining stress.

4. Microcrack Thickness Distribution

Table 1 also lists the distributions of microcrack thickness corresponding to the five different confining conditions. It is clear that with increasing confining stress, the average thickness of the microcracks and their standard deviations are reduced, just like the lengths. Estimated sums of the microcrack thicknesses along diameters of specimen #1 and the unconfined portion of specimen #2 are found to match the measured inelastic lateral deformations of the specimens. This indicates that the inelastic dilatation was caused by the formation of the microcracks, while the deformation in the intact parts of the rock remained elastic. Pore collapse, which is discussed in the next section.

5. Porosity and Volume Changes

The porosities of the elastically deformed specimen #6 (10.31%) and specimens #1 through #5 were carefully measured. The uniaxially compressed specimen (#1) has the greatest final porosity of 13.21%. The partially confined specimen (#2) has a porosity of 11.74% in the unconfined portion and 9.11% in the confined portion. Specimens #3,4 and 5, which were subjected to increasing values of confining stress, show decreases of porosity compared with specimen #6 (Table 1) and volume (Figure 1). The increase in porosity and volume in specimen #1 and the unconfined portion of specimen #2, as shown in figure 1 are due to the opening of microcracks. The decreases in porosities of the confined specimens correspond to pore collapse at high stress. The porosity reduction due to pore collapse more than offsets the overall increase in porosity due to the opening of microcracks.

6. Microcrack Localization and Formation of Shear Bands

In specimen #1 and the unconfined portion of specimen #2, microcracks are found to concentrate in certain regions. The density of microcracks is greater in regions close to free boundaries than in regions near the axes of the specimens. The distribution of microcracks are progressively more homogeneous in specimens #3, 4 and 5, respectively, with several incipient shear bands observed in #3 and #4. Detailed study of the shear bands shows that they consist of many equally spaced extensile microcracks of approximately equal length subparallel to the direction of maximum compression. These microcracks are located inside the specimens, not connected to the free boundary. At the moment of the failure, thin slabs of rock between the extensile microcracks break as suggested by Peng and Johnson (1972) and the shear band propagates into the boundary of the specimens.

CONCLUSIONS

Extensile microcracks in differential compression are generated by many different mechanisms and are oriented subparallel to the maximum compression. The density, length and thickness distributions of the microcracks are controlled by the amount of confining stress to which the specimen is subjected. With zero or low confining stress, the microcracks are concentrated near the surfaces of the specimen. Under high confining stress, the microcracks are more homogeneously distributed. Macroscopic shear bands consist of many extensile microcracks subparallel to the maximum compression. Under uniaxial compression, the dilatation of the specimen is due to the opening of extensile microcracks, even for a clastic, porous rock like Indiana limestone. Under high confining stress, porosity and volume of the specimens are reduced by pore collapse despite microcrack dilatation.

ACKNOWLEDGEMENTS

This work was supported by the Director, Office of Energy Research, Office of Basic Energy Sciences, Division of Engineering, Mathematics, and Geosciences, of the U.S. Department of Energy under contract DE-AC03-76SF00098.

REFERENCES

Ashby, M. F. and S. D. Hallam, 1986. The failure of brittle solids containing small cracks under compressive stress states. *Acta Metall.* Vol. 34, 3: 497-510.

Brace, W.F., B.W. Pauling, and C. Scholz, 1966. Dilatancy in the fracture of crystalline rocks. *J. Geophys. Res.* 71, 16, 3939-3953.

Dey, T. N. and C-Y Wang, 1981. Some mechanisms of crack growth and interaction in compressive rock failure. *Int. J. Rock Mech. Min. Sci.*, 18: 199-209.

Gallagher, J.J., M. Friedman, J. Handin and G.M. Sowers, 1974. Experimental studies relating to microfracture in sandstone, *Tectonophysics*, 21: 203-247.

Hadley, K. 1976. Comparison of calculated crack densities and seismic velocities of Westerly granite. *J. Geophys. Res.* 81: 3484-3494.

Hallbauer, D. K., H. Wagner and N. G. W. Cook, 1973. Some observations concerning the microscopic and mechanical behavior of quartzite specimens in stiff, triaxial compression tests. *Int. J. Rock Mech. Min. Sci.*, 10: 713-726.

Hoek, E. and Z. T. Bieniawski, 1965. Brittle fracture propagation in rock under compression. *Int. J. Fract. Mech.*, 1: 137-155.

Horri, H. and S. Nemat-Nasser, 1985. Compression induced microcrack growth in brittle solids: axial splitting and shear failure. *J. Geophys. Res.* 90, 4, 3105-3125.

Kemeny, J. and N.G.W. Cook, 1987. Crack models for the failure of rocks in compression. *Proc. 2nd Int. Conf. Constitutive Laws Eng. Mat.*, 879-887, Univ. of Arizona, Tucson .

Olsson, W. A. 1974. Microfracturing and faulting in a limestone. *Tectonophysics*, 24: 277-285.

Peng, S. S. and A. M. Johnson, 1972. Crack growth and faulting in cylindrical specimens of Chelmsford granite. *Int. J. Rock Mech. Min. Sci.*, 9: 37-86.

Rao, M. V. M. S. and Y. V. Ramana, 1974. Dilatant behavior of ultramafic rocks during fracture. *Int. J. Rock Mech. Min. Sci. Geomech. Abstr.* 11: 193-203.

Sammis, C. G. and M. F. Ashby, 1986. The failure of brittle porous solids under compressive stress states. *Acta Metall.* Vol. 34, 3:511-526.

Scholz, C. H. 1968. Microfracturing and the inelastic deformation of rock in compression. *J. Geophys. Res.* 73: 1417-1432.

Tapponier, P. and W. F. Brace, 1976. Development of stress-induced microcracks in Westerly granite. *Int. J. Rock Mech. Min. Sci.*, 13: 103-112.

Wawersik, W. R. and C. A. Fairhurst, 1970. A study of brittle rock failure in laboratory compression experiments. *Int. J. Rock Mech. Min. Sci.*, 7: 561-575.

LAWRENCE BERKELEY LABORATORY
TECHNICAL INFORMATION DEPARTMENT
UNIVERSITY OF CALIFORNIA
BERKELEY, CALIFORNIA 94720